Dalton Transactions

COMMUNICATION

View Article Online
View Journal | View Issue

Cite this: *Dalton Trans.*, 2016, **45**, 16148

Received 30th August 2016,
Accepted 12th September 2016

DOI: 10.1039/c6dt03392j

www.rsc.org/dalton

Supramolecular 3d–4f single-molecule magnet architectures†

Sebastian Schmitz,[a] Jan van Leusen,[a] Natalya V. Izarova,[b] Yanhua Lan,[c] Wolfgang Wernsdorfer,[c,d,e] Paul Kögerler*[a,b] and Kirill Yu. Monakhov*[a]

The nanosized self-assemblies $\{[\{Ln^{III}\}\{H_2O\subset Cr^{III}_3Ln^{III}_6\}]_2(H_2O)\}$ (Ln = Dy, 1 and Tb, 2) based on new 3d–4f mixed-metal coordination topologies are formed *via* extensive intramolecular hydrogen bonding that is directed by enclosed water molecules. Compounds 1 and 2 show single-molecule magnet characteristics manifested by hysteresis loops up to 1.6 K (U_{eff} = 8.3 cm^{-1}) and 1 K (U_{eff} = 3.4 cm^{-1}), respectively.

Cooperative non-covalent interactions, in particular hydrogen bonds, are key to hierarchical self-assemblies (*e.g.*, supramolecular polymeric structures).[1] Hydrogen bonding has been shown to affect exchange coupling mechanisms,[2] slow magnetization relaxation,[3] electron tunneling,[4] quantum phase interference,[5] and superconductivity,[6] which has far-reaching implications in the field of molecular electronics and spintronics.[7] Specifically, magnetic compounds with single-molecule magnet (SMM) behavior stand in the focus of these cross-disciplinary efforts. To date, for a great number of SMMs *intermolecular* hydrogen bonds were related to their quantum coherence, Landau–Zener tunneling and exchange-biased quantum tunneling of magnetization,[8,9] whereas discrete SMMs with structurally crucial *intramolecular* hydrogen-bond arrays have not yet been elaborated.

Herein we introduce two charge-neutral 3d–4f molecular magnets whose superstructures with a metal skeleton dimension of *ca.* 17 × 12 Å are maintained by purely intramolecular hydrogen bonds between the self-assembled, nuclearity-distinct molecular entities: $\{[Dy(OAc)_3(H_2O)_3][Dy(H_2O)_3(prop{\cdot}SMe)_3][H_2O\subset Cr_3Dy_6(OAc)_{12}(H_2bda)_3(glyc)_3(ox)_3(prop{\cdot}SMe)_3]_2(H_2O)\}\cdot 12H_2O{\cdot}1.5MeCN$ (**1**) and $\{[Tb(OAc)_3(H_2O)_3][Tb(H_2O)_3(prop{\cdot}SMe)_3][H_2O\subset Cr_3Tb_6(OAc)_{12}(H_2bda)_3(glyc)_3(ox)_3(prop{\cdot}SMe)_3]_2(H_2O)\}\cdot 11.25H_2O{\cdot}1.5MeCN$ (**2**) (Hprop·SMe = 3-(methylthio)propionic acid; H_2bda = *N*-butyldiethanolamine; ox^{2-} = oxalate; $glyc^{2-}$ = glycolate). The most prominent structural motifs in **1** and **2** are $\{H_2O\subset Cr^{III}_3Ln^{III}_6\}$ rings that are linked into supramolecular aggregates *via* a solely hydrogen-bonding H_2O bridge, resulting in linear water triads, capped at their axial ends by additional Ln sites. The $\{H_2O\subset Cr_3Ln_6\}$ entities are further decorated by terminal prop·SMe$^-$ ligands.[10] Both the ligand patterns of the $\{H_2O\subset Cr^{III}_3Ln^{III}_6\}$ rings and the terminal ligand environment of the capping Ln sites differ and thus break the dimer-like symmetry of **1** and **2**.

Compounds **1** and **2** form as octahedrally shaped crystals in one-pot aerobic reactions (see the ESI†) of basic chromium(III) acetate $[Cr_3(OH)_2(OAc)_7]$ and lanthanide(III) acetate tetrahydrate $Ln(OAc)_3{\cdot}4H_2O$, in a 1 : 1 metal ratio with 2.0 eq. of H_2bda in MeCN under reflux, followed by addition of 2.2 eq. of 3-(methylthio)propionic acid (Hprop·SMe). When Hprop·SMe is replaced by 4-(methylthio)phenol (Hphe·SMe) under otherwise identical conditions, slightly larger single crystals of the quasi-isostructural yet thioether-free compound $\{[Tb(OAc)_3(H_2O)_3]_2[H_2O\subset Cr_3Tb_6(OAc)_{15}(H_2bda)_3(glyc)_3(ox)_3]_2\ (H_2O)\}\cdot 10.5H_2O{\cdot}1.5MeCN$ (**3**) can be obtained in low yields. Although not present in the product, Hphe·SMe here is required for isolation of the crystalline material. The presence of oxalates and glycolates in **1–3** is likely linked to aerobic catalytic oxidation of the acetate ligands of the precursors – direct addition of small amounts of oxalic and glycolic acids to the reaction mixtures did not afford the crystalline product. Due to their low solubility, very few oxalate-containing lanthanoid compounds are known (29 CCDC entries; only 6 entries for oxalate-containing complexes of 3d–4f metal ions). Under hydrothermal oxidative conditions, *in situ* oxalate formation has been reported for the decomposition of 2,3-pyrazinedicarboxylic acid in the presence of lanthanoid salts;[11,12] oxalate and glycolate can also

[a]*Institut für Anorganische Chemie, RWTH Aachen University, 52074 Aachen, Germany. E-mail: kirill.monakhov@ac.rwth-aachen.de, paul.koegerler@ac.rwth-aachen.de*
[b]*Jülich-Aachen Research Alliance (JARA-FIT) and Peter Grünberg Institute 6, Forschungszentrum Jülich, 52425 Jülich, Germany*
[c]*Institut Néel (CNRS/UJF UPR2940), 38042 Grenoble cedex 9, France*
[d]*Physikalisches Institut, Karlsruhe Institute of Technology (KIT), 76131 Karlsruhe, Germany*
[e]*Institut für Nanotechnologie, Karlsruhe Institute of Technology (KIT), 76344 Eggenstein-Leopoldshafen, Germany*

†Electronic supplementary information (ESI) available: Experimental details, characterization data, crystallographic data (CIF), and additional tables and figures. CCDC 1487793 (**1**), 1487794 (**2**) and 1487795 (**3**). For ESI and crystallographic data in CIF or other electronic format see DOI: 10.1039/c6dt03392j

be generated similarly *in situ* in the presence of uranium oxynitrate and 1,4-diazabicyclo-[2.2.2]octane.[13] *In situ* production of oxalato-bridged heterometallic compounds by crystallization at room temperature from solutions of 3d metal precursors, lanthanoid acetates and L-ascorbic acid is also known,[14] but it remains unclear if oxalates here originate from the decomposition of L-ascorbic acid, from the oxidation of acetate, or impurities[15] in the employed lanthanoid salts.

The isostructural compounds **1** and **2** crystallize in the trigonal space group *P*31*c* (Table S2, ESI†). The C_3-symmetric supramolecular $\{Ln\cdots\{H_2O\subset Cr_3Ln_6\}\}\cdots(H_2O)\cdots\{\{H_2O\subset Cr_3Ln_6\}\cdots Ln\}$ assemblies in these structures consist of two $\{Ln\cdots\{H_2O\subset Cr_3Ln_6\}\}$ aggregates sandwiching a central water molecule (Fig. 1). In one of the aggregates a $[Ln(OAc)_3(H_2O)_3]$ moiety is situated above the mixed-metal $\{(H_2O)\subset Cr_3Ln_6\}$ ring ($Ln\cdots O_{H_2O}$: *ca.* 4.83 Å for Dy, 4.88 Å for Tb), while the other aggregate is capped by a $[Ln(H_2O)_3(prop{\cdot}SMe)_3]$ unit ($Ln\cdots O_{H_2O}$: *ca.* 4.69 Å for Dy, 4.70 Å for Tb). The capping Ln sites in the $[Ln(H_2O)_3L_3]$ moieties as well as the three central water guests reside on the C_3 axis. While three acetate/thioether ligands of the $[LnL_3(H_2O)_3]$ moieties are directed outwards, the three aqua ligands form hydrogen bonds with oxalate and acetate ligands of the $\{H_2O\subset Cr_3Ln_6\}$ rings.

Each $\{H_2O\subset Cr_3Ln_6\}$ ring is composed of three oxalate-bridged $\{CrLn_2(OAc)_4(H_2bda)(glyc)(prop{\cdot}SMe)\}$ triangles (Fig. 1c), with intra-triangle $Cr^{III}\cdots Ln^{III}$ distances of 3.339(4)–3.360(4) Å for **1** and 3.356(3)–3.374(3) Å for **2**. Intra-triangle Ln⋯Ln distances are 4.100(2)–4.133(2) Å (**1**) and 4.117(1)–4.150(1) Å (**2**); inter-triangle oxalate-bridged Ln⋯Ln pairs range from 6.25–6.28 Å (**1**) and 6.27–6.31 Å (**2**). The Ln_6 substructure is nearly flat, while the outer Cr sites are slightly displaced toward the equator of the entire assembly and each coordinates to one H_2bda *via* its N and two OH sites, two carboxylates in an η^1 mode (OAc^- or $prop{\cdot}SMe^-$), and a glycolate O atom. The bridging OH groups of H_2bda as well as the carboxylates and the glycolate ligands link the Cr to the Ln centers within the $\{CrLn_2\}$ triangles. One of the Ln^{III} ions in $\{CrLn_2\}$ is eight-coordinated bearing the monodentate carboxylate ligand (OAc^- or $prop{\cdot}SMe^-$), the OH group of H_2bda, two oxygens of oxalate, alcoholate and one carboxylic oxygen of glycolate, an O atom of μ_2-bridging the Ln^{III} center with Cr^{III} carboxylate as well as an oxygen atom of the $\mu_2,\eta^1{:}\eta^2$-acetate ligand connecting the two Ln^{III} ions within the $\{CrLn_2\}$ triangle. The second Ln^{III} center is nine-coordinated bearing the chelating acetate ligand instead of the monodentate carboxylate and coordinating two oxygens of the $\mu_2,\eta^1{:}\eta^2$-OAc group instead of a carboxylic glycolate oxygen. The central alcoholate oxygen of $glyc^{2-}$ in $\{CrLn_2\}$ units thus adopts a μ_3-coordination mode, hitherto not observed for this ligand, to connect the three metal ions (see the ESI†). The $prop{\cdot}SMe^-$ ligands occupy two positions within the $\{(H_2O)\subset Cr_3Ln_6\}$ rings that are disordered with acetates: (i) monodentate carboxylates coordinate to the Ln^{III} centers with coordination number 8, and (ii) μ_2-carboxylates connecting Cr^{III} and eight-coordinated Ln^{III} centers. Cr–N (2.10(2)–2.118(16) Å for **1**; 2.089(15)–2.101(17) Å for **2**), Cr–O (1.924(18)–2.025(17) Å for **1**; 1.922(15)–2.019(13) Å for **2**) and the Ln–O bonds are in their usual range (2.235(18)–2.640(20) Å for **1**; 2.259(12)–2.683(14) Å for **2**). The H_2O molecule in the $\{H_2O\subset Cr_3Ln_6\}$ rings is located exactly at the center of the $\{Cr_3Ln_6\}$ rings and seems to template the ring formation through strong hydrogen bonds, with O acceptors of the surrounding glycolate and oxalate ligands (with a minimal O⋯O distance of 2.80(2) Å for both **1** and **2**).

The two $\{H_2O\subset Cr_3Ln_6\}$ rings bind to the water bridge *via* hydrogen bonds to the O sites of proximal glycolate ligands (O⋯O: 2.80(2) Å for **1** and **2**). Thus all three water molecules appear to act as templates, though with an average closest O⋯O distance between the three H_2O molecules of 3.61 Å (**1**)

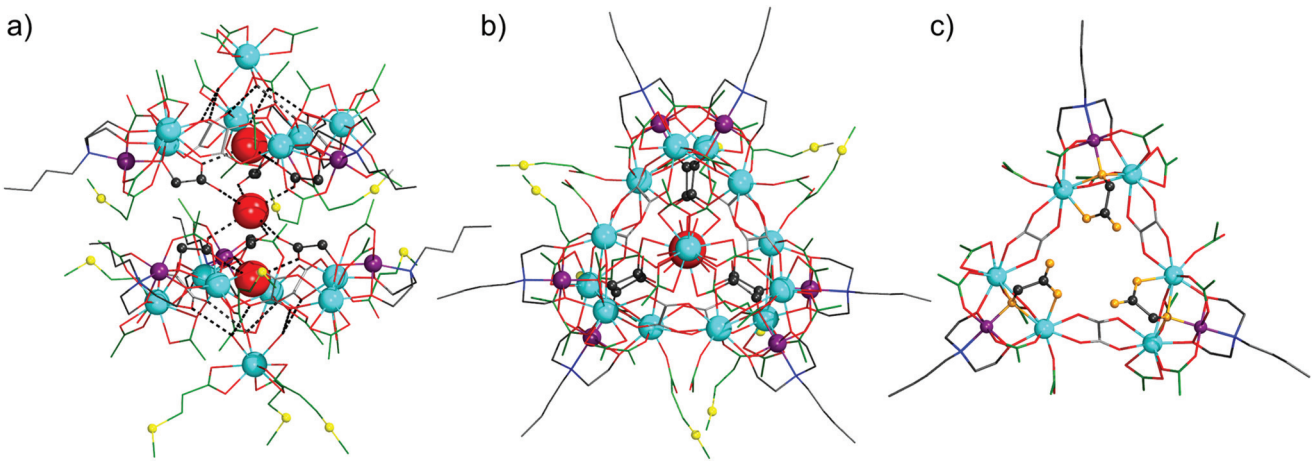

Fig. 1 Side (a) and top (b) views of the solid-state $\{Cr_6Ln_{14}\}$ assembly in **1** and **2**. Ln: light blue, Cr: purple spheres; O: red, S: yellow. The central linear water triad is highlighted by red spheres representing the oxygen atoms. C is colored according to the ligand type: dark gray: H_2bda, light gray: oxalate, green: acetate and $prop{\cdot}SMe^-$, dark gray spheres: glycolate. Hydrogen bonds are indicated as dashed black lines. (c) One of the $\{Cr_3Ln_6\}$ rings, shown without the encapsulated water guest. For disordered acetate and $prop{\cdot}SMe^-$ ligands, only their common O_2C_2 terminus is shown (green). Glyc ligands are highlighted in ball-and-stick mode (C: dark gray, O: orange). All hydrogen atoms are omitted for clarity.

and 3.64 Å (**2**), no direct hydrogen bonding within the $\{H_2O\}_3$ substructure is possible.[16] The $-CH_2-S-Me$ moieties of prop·SMe$^-$ ligands in **1** and **2** are heavily disordered and in part cannot be fully located in single crystal X-ray analyses, despite the fact that several crystals have been measured for every compound. The situation is even more complicated due to the afore-mentioned disorder of prop·SMe$^-$ and OAc$^-$ groups on the $\{H_2O\subset Cr_3Ln_6\}$ rings. Therefore, the exact formulae determined by X-ray analyses (see the ESI†) differ from the disorder-corrected formulae used herein, in particular in a lower content of prop·SMe$^-$. Nevertheless, the sulfur content of 4.3–4.6% determined by elemental analysis in compounds **1** and **2** clearly corresponds to nine to ten S atoms per formula unit. Additional evidence for exactly nine prop·SMe$^-$ ligands in **1** and **2** was found by negative-ion electrospray mass spectrometry. As exemplified by compound **2** containing isotopically pure ^{159}Tb, each $\{CrLn_2\}$ triangle bears one sulfur atom, as indicated by the 100% molecular ion peak assigned to $[CrTb_2(OAc)_3(prop{\cdot}SMe)(H_2bda)(glyc)_3]^-$ (expt. 1062.989 Da, calcd 1063.007 Da; Fig. S3, ESI†).

The unusual structural arrangement of the H-bonded and water-templated $[\{\{Ln^{III}\}\{H_2O\subset Cr^{III}_3Ln^{III}_6\}\}_2(H_2O)]$ assemblies prompted us to investigate the magnetism of **1** and **2** by both direct current (dc) and alternating current (ac) magnetic susceptibility measurements down to 1.8 K and the low-temperature magnetization measured down to 30 mK using micro-SQUID magnetometry. For **1**, the diamagnetism-corrected χ_mT value of 190.45 cm^3 K mol^{-1} at 290 K is slightly below the range of 192.41–208.12 cm^3 K mol^{-1} expected[17] for six high-spin Cr^{III} and 14 Dy^{III} non-interacting centers. This low value hints at the presence of small intramolecular antiferromagnetic exchange interactions. Upon decreasing T, χ_mT gradually increases to a maximum at *ca.* 120 K, subsequently decreases to a minimum at *ca.* 20 K, and finally sharply increases to a maximum of 232.18 cm^3 K mol^{-1} at 2.2 K (Fig. 2a). While both increases indicate ferromagnetic exchange interactions, the decrease may be due to antiferromagnetic interactions and/or due to the thermal depopulation of the m_J substates of the Dy^{III} centers generated by the ligand field. Due to the observation of the low χ_mT value at 290 K, the minimum and the maxima, the exchange interactions are potentially small and of comparable magnitude. The molar magnetization M_m at 2.0 K is a linear function of the applied field B up to *ca.* 0.3 T, and is almost linear for 2–5 T characterized by a, however, distinct different slope reaching $70.8N_A\mu_B$ at 5 T. This value is considerably below the saturation value of *ca.* $158N_A\mu_B$, and may be thus due to antiferromagnetic exchange interactions. However, since the curve is still rising at 5 T, and the states of the Dy^{III} centers are usually mixed m_J states whose compositions can depend on the applied magnetic field,[17] the small magnetization values may be also due to single-ion effects of the Dy^{III} centers. As such, the dc data reveal both antiferromagnetic and ferromagnetic exchange interactions within the compound besides single-ion effects. The ac magnetic susceptibility data at zero bias field show slow relaxation for temperatures below 7.0 K, within the frequency limits of the employed experimental set-up (Fig. 2b). Analyzing the in-phase χ'_m and out-of-phase χ''_m components as a function of the applied frequency f in terms of a generalized Debye expression[18] yields least-squares fits which are depicted as solid lines in Fig. 2b and S5 (ESI†). The distribution of relaxation times (α) suggests the existence of multiple relaxation pathways (α = 0.09–0.46, mean 0.25), and the

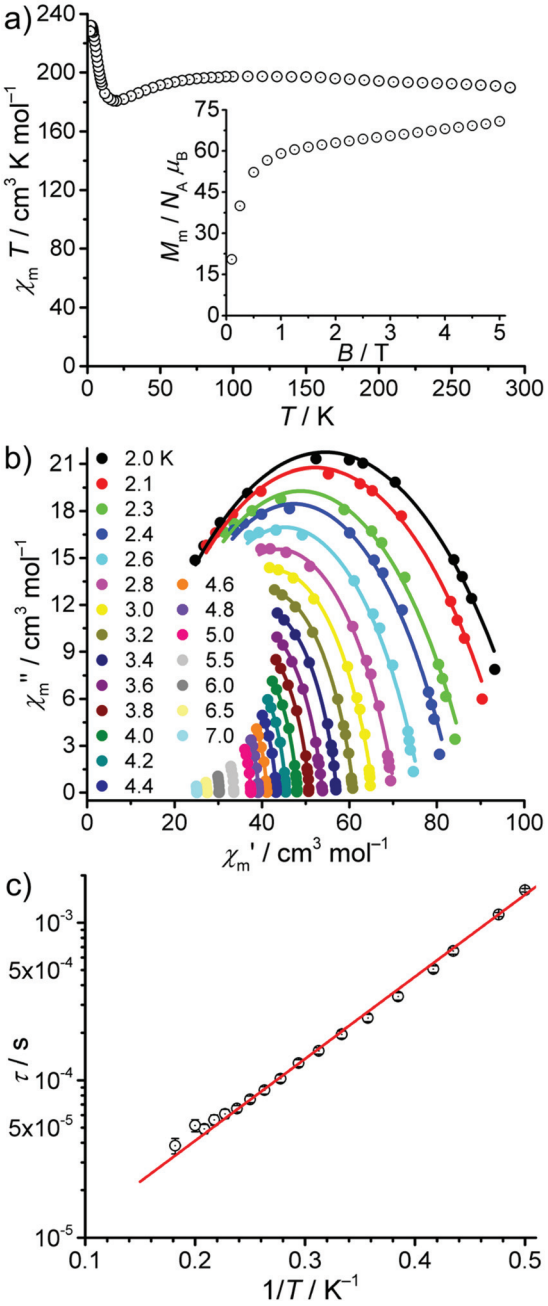

Fig. 2 (a) Temperature dependence of χ_mT at 0.1 T of compound **1**; inset: molar magnetization M_m *versus* applied field B at 2.0 K. (b) Cole–Cole plot for **1** at zero static bias field: experimental data (full circles); fit to the generalized Debye expression[18] (solid lines). (c) Arrhenius plot of the relaxation time τ *vs.* $T^{-}1$ (2.0 K ≤ T ≤ 5.5 K) of **1** (open circles); solid line shows fit to Arrhenius expression.

semi-logarithmic representation of τ *vs.* T^{-1} indicates a mono-exponential relation (Fig. 2c). From this phenomenological perspective, the mono-exponential behavior reveals that the Orbach relaxation process clearly dominates the ac behavior within this temperature range (2.0–7.0 K). We therefore fit the data to a single Arrhenius expression $\tau = \tau_0 \exp[U_{eff}/(k_B T)]$ (k_B: Boltzmann constant) in the range of 2.0–5.5 K yielding the attempt time $\tau_0 = (3.7 \pm 0.3) \times 10^{-6}$ s and the effective energy barrier $U_{eff} = (8.3 \pm 0.2)$ cm^{-1} representing a rather large Orbach relaxation time and a small effective energy barrier.[19]

The magnetic properties of **2** are discussed in detail in the ESI.† The dc susceptibility data reveal antiferromagnetic and ferromagnetic exchange interactions within the compound besides single-ion effects. The magnetic ac data show slow magnetization relaxation for $T \leq 4.6$ K characterized by an attempt time $\tau_0 = (7.5 \pm 0.8) \times 10^{-6}$ s and an effective energy barrier $U_{eff} = (3.4 \pm 0.2)$ cm^{-1}.

A comparison of the magnetic properties of **1** and **2** revealed by measurements down to 2 K shows an overall similar magnetic behavior although there are a few differences: **1** is characterized by more pronounced ferromagnetic exchange interactions than **2**. Both compounds show slow relaxation at low temperatures, and both τ_0 and U_{eff} differ by a factor of roughly **2**.

Low temperature magnetization measurements were carried out on single crystals of **1** and **2** (see the ESI†). The magnetic field is applied parallel to the easy axis of magnetization by using the transverse field method. Open hysteresis loops were observed up to 1.6 K for **1** (Fig. 3) and 1 K for **2** at a sweep rate of 0.14 T s^{-1}, suggesting that **1** has a slightly higher energy barrier as manifested in the ac data. The coercivity fields of the hysteresis loops increase with decreasing temperature and increasing field sweep rates, which is consistent with the phenomenon of superparamagnetic behavior, suggesting that both **1** and **2** behave as SMMs. No step-like feature associated with the occurrence of quantum tunneling of magnetization (QTM) was observed around zero field in the loops for these compounds, indicative of a broadened effect because of the presence of hyperfine coupling of the Tb^{III} and Dy^{III} ions and/or inter- and intramolecular interactions. The width of the loops of **2** around zero field is slightly broader than that of **1**. This can be explained by the nature of the two different types of lanthanoid ions, Tb and Dy (integer spin *vs.* half-integer spin – non-Kramers *vs.* Kramers theorem of spin parity), providing that the direct relaxation process is faster for Tb than for Dy. Similar features were also reported in the hysteresis loops of $DyPc_2$ and $TbPc_2$ double-decker complexes where Pc is a phthalocyaninato ligand.[20] We attempted to extract the relaxation time τ at zero applied field from the decay measurements of the dc magnetization in the temperature range of 1.3–0.03 K. Due to the wide distribution of relaxation processes operative at very low temperatures which coexist with zero-field QTM, no reliable relaxation time could be obtained for both complexes (see the ESI†). The quantum relaxation time approaches toward about 10 s for **1** and 100 s for **2**, confirming the slower zero-field quantum tunneling effect present in the Tb containing complex as indicated in the ac data.

In summary, the formation of quasi-isostructural SMMs **1** and **2** with a layer-like motif is likely induced by templating through cooperative hydrogen bonds of a central, linear triad of water molecules. The $\{Cr_6Ln_{14}(H_2O)_3\}$ aggregates feature several unique structural aspects, from the μ_3-binding mode of glycolate to an unprecedentedly low Cr : Ln[21] ratio of 3 : 7 (reported in CCDC: 1 : 1, 1 : 2, 2 : 3, 3 : 1 and 3 : 2 for Ln = Dy and Tb). The obtained 3d–4f SMMs are reminiscent of quantum-dot 'artificial molecules' exhibiting inter-dot coupling.[22] Moreover, the templating role of water resembles that in polyoxovanadate chemistry (see *e.g.* the archetypal spin-frustrated molecular magnet $[H_2O@V^{IV}_{15}As^{III}_6O_{42}]^{6-}$).[23] Given that the supramolecular aggregates are in principle susceptible to controlled de-aggregation, our next efforts aim at the understanding of the component-dependent dynamic processes inducing and controlling an exchange-biased quantum tunneling in such supramolecular SMM architectures.

This work was supported by an ERC Starting Grant (MOLSPINTRON, 308051). K. Y. M. thanks the Excellence Initiative of the German federal and state governments for an RWTH Start-Up grant. Y. L. and W. W. acknowledge the EU for financial support within the FP7 FET-Proactive project MoQuaS N. 610449 and the Agence Nationale de la Recherche for project MolQuSpin, N. ANR-13-BS10.

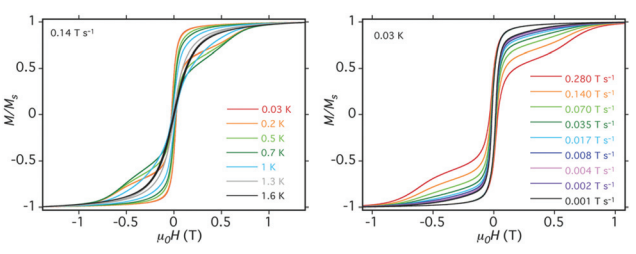

Fig. 3 Temperature dependence (left) and sweep rate dependence (right) of magnetization curves measured as a function of the applied magnetic field at a sweep rate of 0.14 T s^{-1} and at 0.03 K for compound **1**. The magnetization is normalized to its saturation value M_s at 1.4 T.

Notes and references

1 (*a*) C. Rest, R. Kandanelli and G. Fernández, *Chem. Soc. Rev.*, 2015, **44**, 2543; (*b*) A. S. Mahadevi and G. N. Sastry, *Chem. Rev.*, 2016, **116**, 2775.
2 R. D. Willett, C. J. Gómez-García, B. Twamley, S. Gómez-Coca and E. Ruiz, *Inorg. Chem.*, 2012, **51**, 5487.
3 Q. Chen, M.-H. Zeng, Y.-L. Zhou, H.-H. Zou and M. Kurmoo, *Chem. Mater.*, 2010, **22**, 2114.
4 (*a*) T. Nishino, N. Hayashi and P. T. Bui, *J. Am. Chem. Soc.*, 2013, **135**, 4592; (*b*) S. Chang, J. He, A. Kibel, M. Lee, O. Sankey, P. Zhang and S. Lindsay, *Nat. Nanotechnol.*, 2009, **4**, 297.
5 W. Wernsdorfer and R. Sessoli, *Science*, 1999, **284**, 133.

6 I. Errea, M. Calandra, C. J. Pickard, J. R. Nelson, R. J. Needs, Y. Li, H. Liu, Y. Zhang, Y. Ma and F. Mauri, *Nature*, 2016, **532**, 81.

7 (*a*) See the focus issue in *Nat. Nanotechnol.*, 2013, **8**, 377–467; (*b*) D. Xiang, X. Wang, C. Jia, T. Lee and X. Guo, *Chem. Rev.*, 2016, **116**, 4318; (*c*) S. Sanvito, *Chem. Soc. Rev.*, 2011, **40**, 3336; (*d*) D. E. Bürgler, V. Heß, T. Esat, S. Fahrendorf, F. Matthes, C. M. Schneider, C. Besson, K. Yu. Monakhov, P. Kögerler, A. Ghisolfi, P. Braunstein, N. Atodiresei, V. Caciuc and S. Blügel, *e-J. Surf. Sci. Nanotechnol.*, 2016, **14**, 17.

8 See, *e.g.*: (*a*) W. Wernsdorfer, N. Aliaga-Alcalde, D. N. Hendrickson and G. Christou, *Nature*, 2002, **416**, 406; (*b*) S. Hill, R. S. Edwards, N. Aliaga-Alcalde and G. Christou, *Science*, 2003, **302**, 1015; (*c*) W. Wernsdorfer, S. Bhaduri, A. Vinslava and G. Christou, *Phys. Rev. B: Condens. Matter*, 2005, **72**, 214429; (*d*) R. Bagai, W. Wernsdorfer, K. A. Abboud and G. Christou, *J. Am. Chem. Soc.*, 2007, **129**, 12918; (*e*) L. Lecren, W. Wernsdorfer, Y.-G. Li, A. Vindigni, H. Miyasaka and R. Clérac, *J. Am. Chem. Soc.*, 2007, **129**, 5045; (*f*) R. Inglis, L. F. Jones, K. Mason, A. Collins, S. A. Moggach, S. Parsons, S. P. Perlepes, W. Wernsdorfer and E. K. Brechin, *Chem. – Eur. J.*, 2008, **14**, 9117.

9 See also: T. N. Nguyen, W. Wernsdorfer, M. Shiddiq, K. A. Abboud, S. Hill and G. Christou, *Chem. Sci.*, 2016, **7**, 1156 and references cited therein.

10 For peripheral functionalization of metal complexes with thioether groups, see, *e.g.*: (*a*) S. Schmitz, J. van Leusen, A. Ellern, P. Kögerler and K. Yu. Monakhov, *Inorg. Chem. Front.*, 2015, **2**, 1095; (*b*) A. Ghisolfi, K. Yu. Monakhov, R. Pattacini, P. Braunstein, X. López, C. de Graaf, M. Speldrich, J. van Leusen, H. Schilder and P. Kögerler, *Dalton Trans.*, 2014, **43**, 7847; (*c*) A. Cornia, M. Mannini, P. Sainctavit and R. Sessoli, *Chem. Soc. Rev.*, 2011, **40**, 3076.

11 P. C. R. Soares-Santos, L. Cunha-Silva, F. A. A. Paz, R. A. S. Ferreira, J. Rocha, L. D. Carlos and H. I. S. Nogueira, *Inorg. Chem.*, 2010, **49**, 3428.

12 K. E. Knope, H. Kimura, Y. Yasaka, M. Nakahara, M. B. Andrews and C. L. Cahill, *Inorg. Chem.*, 2012, **51**, 3883.

13 K. E. Knope and C. L. Cahill, *Inorg. Chem.*, 2007, **46**, 6607.

14 A. S. Dinca, S. Shova, A. E. Ion, C. Maxim, F. Lloret, M. Julve and M. Andruh, *Dalton Trans.*, 2015, **44**, 7148.

15 J. E. Tackett, *Appl. Spectrosc.*, 1989, **43**, 490.

16 R. Ludwig, *Angew. Chem., Int. Ed.*, 2001, **40**, 1808.

17 H. Lueken, *Magnetochemie*, Teubner Verlag, Stuttgart, 1999.

18 K. S. Cole and R. H. Cole, *J. Chem. Phys.*, 1941, **9**, 341.

19 (*a*) L. R. Piquer and E. C. Sanudo, *Dalton Trans.*, 2015, **44**, 8771; (*b*) D. N. Woodruff, R. E. P. Winpenny and R. A. Layfield, *Chem. Rev.*, 2013, **113**, 5110.

20 (*a*) N. Ishikawa, M. Sugita and W. Wernsdorfer, *Angew. Chem., Int. Ed.*, 2005, **44**, 2931; (*b*) N. Ishikawa, M. Sugita, T. Ishikawa, S. Koshihara and Y. Kaizu, *J. Phys. Chem. B*, 2004, **108**, 11265.

21 For other recent Cr^{III}–Ln^{III} SMMs, see: (*a*) S. K. Langley, D. P. Wielechowski, N. F. Chilton, B. Moubaraki and K. S. Murray, *Inorg. Chem.*, 2015, **54**, 10497; (*b*) S. K. Langley, C. M. Forsyth, B. Moubaraki and K. S. Murray, *Dalton Trans.*, 2015, **44**, 912.

22 (*a*) T. H. Oosterkamp, T. Fujisawa, W. G. van der Wiel, K. Ishibashi, R. V. Hijman, S. Tarucha and L. P. Kouwenhoven, *Nature*, 1998, **395**, 873; (*b*) C. Livermore, C. H. Crouch, R. M. Westervelt, K. L. Campman and A. C. Gossard, *Science*, 1996, **274**, 1332; (*c*) R. H. Blick, R. J. Haug, J. Weis, D. Pfannkuche, K. Klitzing and K. Eberl, *Phys. Rev. B: Condens. Matter*, 1996, **53**, 7899.

23 K. Yu. Monakhov, W. Bensch and P. Kögerler, *Chem. Soc. Rev.*, 2015, **44**, 8443 and references cited therein.